Mechanics and Chemotaxis in the Morphogenesis of Vascular Networks

A. Tosin, D. Ambrosi, L. Preziosi

Politecnico di Torino, Dipartimento di Matematica
Corso Duca degli Abruzzi, 24 - 10129 Torino, Italy

Abstract

The formation of vascular networks *in vitro* develops along two rather distinct stages: during the early migration-dominated stage the main features of the pattern emerge, later the mechanical interaction of the cells with the substratum stretches the network. Mathematical models in the relevant literature have been focusing just on either of the aspects of this complex system. In this paper, a unified view of the morphogenetic process is provided in terms of physical mechanisms and mathematical modeling.

Key words: vascular networks, vasculogenesis, chemotaxis, cell traction, elasticity

1 Introduction

When cultured *in vitro* in a suitable environment, Endothelial Cells (ECs) are able to organize themselves to form capillary-like networks. This characteristic is shared by several cell lines [24]; particularly interesting is the observation that also melanoma cells seem to have the capability to form capillary-like structures by themselves which favor their growth [12,17]. The details of the morphogenetic process may differ depending on the specific experimental setting at hand (see [2] for an extended review on this issue).

Mathematical literature on the subject is quite partitioned into two mainstreams, that in essence correspond to two different explanations for the basic mechanism of intercellular communication leading to pattern formation. The

earlier thread is due to Murray, Oster and coworkers (see [16,18] and other papers referenced therein). They focus on the mechanical interactions between cells and Extra-Cellular Matrix (ECM) that occur when ECs adhere to the underlying layer and stretch it. These Authors observe that the tensional field caused by the cell pulling on the substratum creates a local indirect information about the concentration of the cells themselves on the surrounding surface. They therefore assume that ECs detect the stress field of the layer and move on the surface along the tensional lines (*mesenchymal motion*). Cell organization in soft media due to active mechanosensing has been confirmed by a number of experiments reported in the recent literature too (see [3] and the references therein). As the tension depends on the number of pulling cells, the migrating ones move toward regions of larger cellular density. Qualitative analysis and numerical integration of the set of partial differential equations corresponding to the mathematical formalization of this idea demonstrate that network-like structures actually form on the basis of this assumption.

However, recent experimental works [21] have pointed out that before mesenchymal motion activates cells undergo a faster *amoeboid-type migration* driven by chemical factors such as VEGF (Vascular Endothelial Growth Factor). During this stage a draft of the final network emerges, although it exhibits itself in the final form only after the stretching process. Even more important, laboratory investigations demonstrate that a characteristic mesh size independent of the number of cells exists, provided the latter are neither too many nor too few in order for the morphogenetic process to start up. Conversely, the conjecture that the network forms just during the mesenchymal migration does not predict the existence of any characteristic length, so that the final mesh size would be dictated essentially by the initial conditions. The key role of the VEGF in network formation is also demonstrated by the experiment of Helmlinger *et al.* [11]. They study the network-like structures formed by human umbilical cells in a sandwich, where the stretching of the substratum is inhibited. The morphology of the pictures in their paper exhibits a characteristic length, but the cords are quite thicker and less rectilinear than in usual ECM assays (see, *e.g.*, [24,23,19]), thus suggesting again the fundamental role of chemical intercellular communication in this process.

To obviate these difficulties of the theory, some Authors have recently proposed mathematical models in which the chemotactic interaction is the real driver of network formation [1,6]. This assumption is supported by the observation that exogenous saturation of the signaling of some VEGF inhibits the networking. The mathematical model identifying the chemical signaling as the key mechanism of vasculogenesis predicts a characteristic length of the mesh size which is in good agreement with the experiments.

Aim of this paper is to provide a unified view of the whole morphogenetic process of vascular networks, including both amoeboid and mesenchymal migra-

2

tion. ECs and ECM are described as a two-layers system in which the vertical dimension can be neglected. The two layers are shallow continuous bodies that obey standard force balance equations including an interaction term, which couples the motion of the cells and the substratum. This simple setting allows to include in the description both the (independent) reorganization of the cells according to chemotactic signaling and the (coupled) stretching of the gel. This approach provides a satisfactory unified framework for the vasculogenic process at all stages, and the numerical simulations suggest that a stable steady solution should exist in a physically significant range of parameters.

This paper is divided into six sections. After this Introduction, Section 2 is devoted to summarize the experimental facts of a particular biological assay, while in Section 3 a new mathematical model is illustrated accounting for both chemotactic and mechanical aspects of the vasculogenic process. This model is discussed and compared with the existing ones in Section 4, and in Section 5 the results of the related numerical simulations are shown and commented. Finally, Section 6 briefly sketches some research perspectives.

2 Experimental facts

In this section we specifically refer to the experiments by Serini *et al.* [21]. Generalization of the dynamics illustrated here to other vasculogenesis assays (involving different cells or different substrata) should be done with great care.

Serini and his coworkers use a Petri dish coated with an amount of Matrigel, a surface which favors cell motility thanks to biochemical characteristics similar to those of living tissues. Human ECs from large veins (*e.g.* HUVEC, Human Umbilical Vein ECs) or from adrenal cortex capillaries are dispersed in a physiological solution which is poured on the top of the Matrigel. After sedimentation due to gravity, cells move on the horizontal surface of the substratum giving rise to a process of aggregation and pattern formation.

If the proper number of cells is used (cell density ranging from 100 to 400 cell/mm^2), a vascular-like network develops. The entire process lasts 12-15 hours and evolves according to the following steps:

i) in the first few hours (2-3 hours) ECs migrate independently, keeping a round shape (Figures A.1a-b). In this phase, cell motion is of amoeboid type (see, *e.g.*, [4,25,26]); it is faster than later motion and shows a high persistence [21,22]. Intriguingly, an indirect confirmation of the existence of this amoeboid stage can be deduced also from the experiment of Ferrenq *et al.* [5]: they measure the traction exerted by the cells on the gel, and almost no action is registered in the first two hours, a stage that they call "latency

3

time" and that can probably be interpreted in terms of amoeboid motion;

ii) the cells, attracted toward regions with higher cellular density, attach to the neighboring ones and, if possible, form a continuous multicellular network (Figure A.1c);

iii) the cells take a more elongated shape. Their motion becomes mesenchymal, they anchor themselves to the ECM, and, acting on the adhesion sites, start pulling the substratum and the other cells. The network slowly moves as a whole, undergoing a slow thinning process (Figure A.1d), probably driven by the stress field generated by mutual tractions;

iv) in the final phase, individual cells differentiate and fold up to form the lumen of the capillary, so that the formation of a capillary-like network takes place along the lines of the previously formed two-dimensional structure as described in [9,13].

A movie of an experiment can be viewed at the EMBO web site[1] as a supplementary material to the paper by Serini *et al.* [21].

Two transitions are observed at low and high cell densities. The former is a percolative transition which occurs below the critical threshold of 100 cells/mm^2 and gives rise to groups of disconnected structures. This transition is analyzed in detail in [6]. The latter gives rise to thicker cords, and for very high cell density (say above 400 cells/mm^2) to the formation of a continuous carpet of cells with holes or *lacunae*.

Note that the experimental evidences reported in the Introduction demonstrate the role of the chemotactic interaction in pattern generation, but there is no reason to restrict this effect to the amoeboid stage; it seems instead reasonable that also the apparent mesh remodeling occurring at later times be driven by a joint chemomechanical interaction.

3 The two-layers model

In our mathematical model deduction, we regard ECs and ECM as two continuous shallow layers. In the experiments, the substratum has a horizontal length of the order of 1 mm, and a thickness of the order of 10 μm: this suggests that a two-dimensional mathematical modeling of the system could be sufficient to capture the main characteristics of the phenomenon.

Remark. In order to roughly estimate the depth into the ECM thickness at which the superficial action of the cells is influential, we observe that the main balance is between the cell traction τ and the shear stresses τ_{xz}, τ_{yz}

---

[1] `http://embojournal.npgjournals.com`

4

of the substratum. Denoting by U the order of magnitude of the horizontal displacement of the cells, and by Z the typical length scale of the vertical displacement of the ECM, we have therefore the relation $\mu U / Z \sim \tau$, that yields in turn

$$Z \sim \frac{\mu U}{\tau},$$

where μ is the Lamé elastic constant of the substratum. From experimental measurements [7,19], it is known that

$$\mu \sim 10^3 \text{ Pa}, \quad U \sim 10 \ \mu\text{m}, \quad \tau_{\text{max}} \sim 10^2 \text{ Pa},$$

hence $Z_{\text{max}} \sim 10^2 \ \mu\text{m}$ is obtained. Since this value is much higher than the actual thickness of the substratum used in the experiments mentioned above, we conclude that the action of the cells is not confined in a thin layer under the top surface of the ECM, but it influences the whole thickness of the latter. This observation supports the possibility to adopt a 2D mathematical modeling of the substratum via an averaging process of the corresponding 3D equations (see below).

We model the bio-mechanical system illustrated in the previous section as a set of two 2D layers that move and stretch over each other, experiencing mutual interaction forces in the horizontal plane. The unknowns of the problem are therefore the horizontal displacement of the substratum $\mathbf{u}(\mathbf{x}, t)$ and the horizontal velocity field of the cells $\mathbf{v}(\mathbf{x}, t)$, associated to a density field $\rho(\mathbf{x}, t)$, where $\mathbf{x} = (x, y)$. In the experimental papers, the cellular density is usually referred to in terms of number of cells per unit area; here, instead, ρ denotes the mass of the cellular matter per unit surface.

The momentum balance for the ECM reads

$$-\nabla \cdot \mathbb{T}_s = \boldsymbol{\sigma}, \tag{1}$$

where $\mathbb{T}_s$ is the (two-dimensional) Cauchy stress tensor of the substratum and $\boldsymbol{\sigma}$ is the force per unit surface occurring between the ECM and the cells.

The mass conservation and the momentum balance equations for the cell density field are given by

$$\frac{\partial \rho}{\partial t} + \nabla \cdot (\rho \mathbf{v}) = 0, \tag{2}$$

$$\frac{\partial}{\partial t}(\rho \mathbf{v}) + \nabla \cdot (\mathbf{v} \otimes \rho \mathbf{v}) - \nabla \cdot \mathbb{T}_c = -\boldsymbol{\sigma} + \rho \mathbf{f}_c. \tag{3}$$

No source is considered at the right-hand side of Equation (2), the typical time of an experiment being much smaller than the duplication time of the cells. In some experiments possible detachments of the cells from the substratum are reported [23], but we disregard them as higher order effects.

The forces appearing in Equation (3) have a different physical nature: the stress tensor $\mathbb{T}_c$ accounts for internal forces in the cell layer; $\boldsymbol{\sigma}$ is an external force for the cellular layer, that reads as internal for the whole system; the bulk force per unit mass $\mathbf{f}_c$ accounts for cell-cell interaction via the chemotactic signaling.

The first and second terms in the left-hand side of Equation (3) are formally identical to the usual material acceleration of a continuum. However, this does not mean that cells behave like particles, the Galilean inertia being definitely negligible in this context. Rather, the nonlinear term at the left-hand side of Equation (3) accounts instead for persistence in cell motion, *i.e.*, for their "inertia" in changing their direction [4,22]. Far from claiming that this is the unique way to model persistence in a continuous modeling of the cellular matter; we just remark that persistence is an essential ingredient to design a mathematical model of cell networking, and this is a possible choice that works.

The chemotactic interaction is introduced in the present context as a surface force that tends to aggregate the cells, driving them along the direction of the chemical gradient:

$$\mathbf{f}_c = \beta \nabla c.$$

Furthermore, the balance of the chemotactic factor, characterized by the concentration field per unit volume $c(\mathbf{x}, t)$, is governed by a standard reaction-diffusion equation

$$\frac{\partial c}{\partial t} - D \Delta c = \alpha(\rho)\rho - \frac{c}{\tau},$$

where D is the diffusion coefficient. The quantities τ and $\alpha(\rho)$ are the half-life and the production rate of the chemoattractant factor and are due to the degradation process and the production by cells, respectively. In this paper we assume that long-range chemotactic communication is switched off when cells reach an aggregate state; therefore, the function $\alpha(\rho)$ should be characterized by the following properties:

i) a finite maximum for $\rho = 0$ and a monotone decreasing behavior for $\rho > 0$, in order to mimic the diminishing in the chemoattractant production as the cellular matter becomes more aggregate;

ii) $\alpha(\rho) \to 0$ when $\rho \to +\infty$ rapidly enough in order for the chemoattractant production to vanish when cells come in a sufficiently packed configuration.

Mechanical Constitutive Equations

The extracellular matrix is known to exhibit a viscoelastic mechanical behavior, characterized by relaxation times of the order of 100 seconds at most. Therefore in the present context, dealing with a process that lasts hours, we

can straightforwardly neglect the viscoelastic effects and suppose that the Cauchy stress tensor depends on the strain tensor:

$$\mathbb{T}_s = \mathbb{T}_s(\nabla \mathbf{u}). \tag{4}$$

In particular, in the following we assume that the displacement of the ECM is sufficiently small that linear elasticity applies. Note that because of the previously mentioned two-layers hypothesis, Equations (1) and (4) have to be understood within the framework of a plane problem of elastostatics, assuming in particular a state of *plane stress*. Regarding the analytical derivation of the proper equations for such a problem in terms of the displacement $\mathbf{u}$ of the substratum [2], we specifically refer to [10].

The cellular layer has been effectively modeled in other papers as an elastic fluid [1,6,21]:

$$\mathbb{T}_c = -p(\rho)\mathbb{I},$$

where $\mathbb{I}$ is the identity 2×2 matrix, and $p(\rho)$ is a function such that its gradient is negligible for small density and strongly increases when a density near to the close packing of the cells is approached.

The interaction force $\boldsymbol{\sigma}$ between the cell layer and the ECM drives the deformation of the latter. It is not yet clear which mechanism activates the strong cell adhesion on the ECM that causes the motion to switch from amoeboid to mesenchymal. At the present stage we can just conjecture that amoeboid motion stops when cells come in "sufficient" contact, *i.e.*, when the network stretch starts up. If at a given time a cell anchors at a point $\mathbf{x}_0$ of the substratum and then moves to $\mathbf{x}_1$, while the substratum is simultaneously stretched so as the point $\mathbf{x}_0$ moves to $\mathbf{x}_2$, a force between the cell and the substratum arises, that we can assume elastic and in particular proportional to $\mathbf{x}_2 - \mathbf{x}_1 = \mathbf{u} - \mathbf{u}_c$, where $\mathbf{u} = \mathbf{x}_2 - \mathbf{x}_0$ and $\mathbf{u}_c = \mathbf{x}_1 - \mathbf{x}_0$. This ideally means that the cell and the ECM are connected by a spring which obeys the linear Hooke's law, $\mathbf{x}_2 - \mathbf{x}_1$ being its elongation (Figure A.1d). Then we set

$$\boldsymbol{\sigma} = -\kappa(\rho)\left(\mathbf{u} - \mathbf{u}_c\right), \tag{5}$$

where $\kappa(\rho)$ vanishes for low density. According to Equation (5), the cells stick to the substratum at the initial time, quite a rough modeling of the real transition from amoeboid to mesenchymal motion observed in the experiments. We just remark that this unsatisfactory modeling point is not a mathematical flaw, rather it is due to a still incomplete biological knowledge.

---

[2] As a matter of fact, the analytical derivation of the equilibrium equations for a linear elastic plane stress problem involves an averaging process of the corresponding 3D equations along the thickness of the substratum. Therefore, $\mathbf{u}$ should be more correctly interpreted as the *average* horizontal displacement of the ECM.

The reader is referred to Appendix A for the specific form of the functions $p(\rho)$, $\kappa(\rho)$ used in the numerical simulations, as well as of the function $\alpha(\rho)$ introduced above.

4 Discussion of the mathematical model

The balance equations and the constitutive equations stated in Section 3 yield the following differential system:

$$\frac{\partial \rho}{\partial t} + \nabla \cdot (\rho \mathbf{v}) = 0, \tag{6}$$

$$\frac{\partial}{\partial t}(\rho \mathbf{v}) + \nabla \cdot (\mathbf{v} \otimes \rho \mathbf{v}) + \nabla p(\rho) = \kappa(\rho)\,(\mathbf{u} - \mathbf{u}_c) + \beta \rho \nabla c, \tag{7}$$

$$-\frac{E}{2(1+\nu)}\Delta \mathbf{u} - \frac{E}{2(1-\nu)}\nabla(\nabla \cdot \mathbf{u}) = -\kappa(\rho)\,(\mathbf{u} - \mathbf{u}_c), \tag{8}$$

$$\frac{\partial c}{\partial t} - D\Delta c = \alpha(\rho)\rho - \frac{c}{\tau}, \tag{9}$$

where E and ν denote the Young modulus and the Poisson ratio of the substratum respectively, supplemented by the compatibility condition:

$$\frac{d\mathbf{u}_c}{dt} = \mathbf{v}. \tag{10}$$

When $\kappa \equiv 0$ no interaction exists between the layers, the dynamics of ECs and ECM are decoupled and one partially recovers the chemotactic model by Ambrosi *et al.* [1].

The evolution of the system predicted by the set of Equations (6)-(10) is depicted in Figure A.1.

[Fig. 1 about here.]

After the random seeding of the cells (Figure A.1a), the chemotactic field is set up. Cells start moving along the chemical gradient, driven by the chemotactic force (Figure A.1b). The persistence term in the equations makes the cellular matter preserve its initial direction of motion, which is not in general strictly directed toward larger density points. This delay in the cellular response causes cells not to cluster; they instead empty the lower density regions, forming a density pattern with spatial characteristics dictated by the typical length $\ell \approx \sqrt{D\tau}$ (see [1]). The traction between the cellular layer and the gel starts acting when a sufficiently large density is locally obtained, so that $\kappa(\rho)$ is not negligible. At this stage (Figure A.1c) cells hang on and stretch the substratum. In Figure A.1d is pictorially shown the spring ideally connecting the two layers. Cell-ECM adhesiveness and mechanical characterization of the substratum are two distinct physical effects that are duly incorporated

into the model by different terms. The function $\kappa(\rho)$ accounts for adhesiveness, a mutual characterization of cells and ECM; on the other hand, E and ν measure the stiffness of the material composing the substratum.

The final scenario can be understood by summing up Equations (7) and (8) at the steady state, after obtaining c formally from Equation (9):

$$-\frac{E}{2(1+\nu)}\Delta\mathbf{u} - \frac{E}{2(1-\nu)}\nabla\left(\nabla\cdot\mathbf{u}\right) + \nabla p(\rho) =$$
$$= \beta D\rho\nabla\left[\left(\frac{1}{D\tau} - \Delta\right)^{-1}\alpha(\rho)\rho\right]. \quad (11)$$

If the system is far from the percolative transition threshold (low ρ), the intercellular pressure is negligible and Equation (11) accounts for the balance between the aggregative tendency of the anchored cells (r.h.s.) and the elastic response of the ECM (l.h.s.). The non-local operator at the right-hand side of Equation (11) acts as a filter, damping the wavelengths larger than $\sqrt{D\tau}$ (see [1]).

Equation (11) is very similar to the force balance equation written by Murray and coworkers in [16] for the gel-cell system. Their seminal work has pioneered a class of mathematical models (see also [15,19]) describing the *in vitro* vasculogenesis in terms of mechanical interactions between ECs and ECM. In the following, we shall briefly sketch the main analogies and differences between these models and the general formulation illustrated in the present section.

i) Murray and coworkers do not write a differential equation for the velocity $\mathbf{v}$ of the cells, and therefore they do not account for persistence. In their model, the movement of the cells is due to the superposition of a diffusive "matrix guided" motion (a movement biased toward the directions of the principal strains of the ECM), and the drift velocity $\frac{\partial\mathbf{u}}{\partial t}$. Namy and coworkers [19] add to this framework some other more sophisticated effects, such as cell sensitivity to ECM density gradient (*haptotaxis*) and long-range interactions in ECM stretching due to the fibrous nature of the substratum.

ii) The models presented in [15,16,19] consider the spatial reorganization of the ECM mass induced by cellular tractions as one of the main factors for the formation of the networks; consequently, they all include a balance equation for the ECM density, a quantity that here plays no specific role.

iii) Murray and coworkers write a force balance equation for the gel-cell system very similar to Equation (11), including the shear stress of the Petri dish on the ECM. We do not explicitly take into account this contribution, but we recover otherwise its main effect, which essentially consists in filtering out the rigid motion of the gel (see Section 5).

iv) In general, chemotaxis and all the related effects are completely neglected. Actually, Manoussaki [15] acknowledges a theoretical role to chemotactic

9

factors, and indeed she includes them in her model by a diffusion equation analogous to Equation (9); however, they are disregarded in the numerical simulations. Note that if no diffusion of chemoattractant occurs, then the non-local operator at the right-hand side of Equation (11) disappears and the density field ρ directly drives the stretch of the ECM, without the *filtering* operated by the chemical field. No characteristic length independent of the initial conditions should then be observed in such a case.

5   Quantitative Results

The model illustrated in the previous sections has been converted in a dimensionless form (see Appendix A), and then numerically integrated in the reference square with a spatial resolution of 128×128 nodes. Numerical simulations have been performed using this set of non-dimensional parameters and functions:

$$\nu = 0.2, \qquad \beta^* = 0.02, \qquad \eta^* = 50$$

$$k^*(\rho^*) = 0.2\rho^*, \qquad \alpha^*(\rho^*) = \frac{30}{1 + 0.2\rho^{*2}}.$$

Periodic boundary conditions have been prescribed for all the state variables; furthermore, the following non-dimensional initial conditions have been imposed:

$$\rho^*(\mathbf{x}^*,\, 0) = \frac{1}{2\pi r^{*2}} \sum_{j=1}^{M} \exp\left(-\frac{|\mathbf{x}^* - \mathbf{x}_j^*|^2}{2r^{*2}}\right),$$

$$\mathbf{v}^*(\mathbf{x}^*,\, 0) = \mathbf{u}^*(\mathbf{x}^*,\, 0) = c^*(\mathbf{x}^*,\, 0) = 0.$$

The initial condition on the cellular density corresponds to a set of M Gaussian bumps whose amplitude is assumed to be of the order of the non-dimensional average cell radius r^* (the physical cell radius being about $r = 20\,\mu\mathrm{m}$), centered randomly in $\mathbf{x}_j^*$, $j = 1, \ldots, M$, with a uniform distribution over the square.

After an implicit discretization in time by a backward Euler scheme, the parabolic equation (9) has been discretized in space by a spectral method and solved by the Fast Fourier Transform algorithm. The elliptic non-evolutive equation (8) has been discretized by a spectral method nested in an iterative procedure to take into account the spatially non-constant coefficient term $-\kappa(\rho)\mathbf{u}$ at the right-hand side. Note that the presence of periodic boundary conditions on $\mathbf{u}$ causes the substratum not to be constrained in any way. Rigid motions are removed from the set of possible motions by imposing that the

amplitude of the Fourier mode corresponding to the null wavenumber vanishes. Equations (6) and (7) constitute a non linear hyperbolic system with source term; the right-hand side has been discretized by a Godunov method, while a simple centered discretization has been applied to the left-hand side. The displacement field of the cells $\mathbf{u}_c$ (Equation (10)) is numerically obtained integrating in time the velocity field $\mathbf{v}$ by a first order finite difference scheme.

Figure A.2 shows a comparison between the experimental pictures of the vascular network formation as obtained by videomicroscopy (a) and as predicted by the model (b). The non-dimensional time is listed in the left column. The geometrical properties of the network shown in Figure A.2b are very similar to the experimentally observed ones.

[Fig. 2 about here.]

Figure A.3 shows the influence of cellular adhesiveness to the substratum on the formation of vascular networks as predicted by the model. If the adhesiveness is too strong, no network forms (Figure A.3c). As the adhesiveness is the macroscopic result of microscopic chemical bonds that occur between each cell and the ECM, the stronger the bonds are, the more inhibited the movement of the cells is. On the other hand, for too weak adhesiveness the chemotactic action becomes prevalent, and one can observe a rapid formation of cords that do not reach a steady state (Figure A.3b), like in the mathematical model proposed by Ambrosi *et al.* [1]: cells continue to pack and they finally cluster in big mounds. Only when chemotactic attraction and mechanical interactions balance does a stable network structure form (Figure A.3a). In particular, numerical simulations show that the networking is essentially allowed or inhibited by the relative magnitude of the parameters β^* and κ^*, that, up to non-dimensionalisation, account for the intensity of the intercellular chemotactic signaling and for the stiffness of the ECs-ECM adhesion respectively. Conversely, the morphogenetic process is virtually independent of the Young modulus E of the substratum, which instead affects mainly the magnitude of the ECM deformation and displacement from the unstressed configuration (see Appendix A).
As mentioned in Section 2, at later times cells differentiate in tubular structures and, consequently, the present two-dimensional model no longer applies.

[Fig. 3 about here.]

Figure A.4a shows the contour plot of the ECM stress tensor norm $\|\mathbb{T}_s\|$ at the final stage of the network formation, the corresponding cellular density being represented in Figure A.4b. We use the definition

$$\|\mathbb{T}_s\|^2 := \operatorname{trace}\left(\mathbb{T}_s^T \mathbb{T}_s\right),$$

so that $\|\mathbb{T}_s\|$ gives a measure of the magnitude of the stress affecting the

substratum due to the traction exerted by the cells. Figures A.4c and A.4d are magnifications of the previous pictures referred to a particular area of the domain. Numerical simulations suggest that most stress is concentrated in thin strips edging the cords or surrounding the cell density holes.

[Fig. 4 about here.]

In Figure A.5 the magnitude of the spatially averaged chemotactic and elastic forces are compared. The plot shows that in the early times of the simulation the chemotactic force grows more rapidly than the elastic one, so that in the first period (say about $0 \leq t \leq 3$) chemotaxis dominates. Later the elastic force grows, until a substantial equilibrium is reached.

[Fig. 5 about here.]

6 Final remarks

This paper is based on the observation that, in vascular network formation, migration and traction are different programs that an individual cell is able to execute. We conjecture that the beginning of either program is dictated by the local cell density, which leads the system to an amoeboid or mesenchymal regime.

In our opinion persistence, chemotaxis, and mechanics provide complementary description of *in vitro* vasculogenesis experiments. Persistence and endogenous chemotaxis are essential ingredients in the early, migration dominated stages of network formation. They govern the size of the capillary structure via the diffusion coefficient D and the chemoattractant half-life τ. The predicted average size of the fully formed network structures is $\ell \approx \sqrt{D\tau}$, in good agreement with phenomenological observations *in vivo* and measurements *in vitro*. Intriguingly, this is in agreement with the observation that mice lacking heparin-binding isoforms of VEGF-A, characterized by smaller diffusivity, form vascular networks with a larger mesh [20].

The main role of the mechanical interactions between ECs and ECM is to stabilize the structures. In the purely chemotactic model by Ambrosi *et al.* [1], the cell-cell interaction is confined to normal stresses only, given by the intercellular pressure $p(\rho)$. Although this is a sufficient condition in order for the solution $\rho(\mathbf{x}, t)$ not to blow-up in time, as proved by Kowalczyk in [14], it does not guarantee the preservation of the network morphology under shear perturbations. Instead, the anchorage of the cells to the substratum, which is able to sustain not only normal stress but also shear stress, provides stability to the structures.

Of course, some issues remain to be investigated in the future. For instance, some experimental movies show that the ECM can be locally stretched at a high ratio, including not negligible vertical displacements. This behavior would prevent from using a linear elastic model and also the "thin layer" approximation could not apply.

A natural generalization of the present work would be to extend the mathematical model to three-dimensional cell migration. Unfortunately, recent experimental investigations suggest that a pure transposition of the theory would be just an academic exercise. In fact, 3D migration of the cells occurs in a very different way [4,26]: cells essentially thread themselves and climb fibers of the ECM. The motion is always mesenchymal, and fibers orientation plays a fundamental role. It remains an open question to what extent the achievements in the understanding of the 2D vasculogenesis will be helpful to address the real three-dimensional setting.

Acknowledgments

A   Non-dimensional form of the equations

Let us introduce the following non-dimensional variables:

$$\mathbf{x}^* := \frac{\mathbf{x}}{\ell}, \quad t^* := \frac{t}{T}, \quad \rho^* := \frac{\rho}{\rho_0}, \quad c^* := \frac{c}{C}$$

where ℓ, T, ρ_0, C are typical values of length, time, cell density and chemoattractant concentration, respectively.
Choosing $\ell = \sqrt{D\tau}$ (as suggested by Equation (9) at the steady state) and

$T = \tau$ yields the non-dimensional system

$$\frac{\partial \rho^*}{\partial t^*} + \nabla^* \cdot (\rho^* \mathbf{v}^*) = 0$$

$$\frac{\partial}{\partial t^*}(\rho^* \mathbf{v}^*) + \nabla^* \cdot (\mathbf{v}^* \otimes \rho^* \mathbf{v}^*) + \nabla^* p^*(\rho^*) = \kappa^*(\rho^*)(\mathbf{u}^* - \mathbf{u}_c^*) + \beta^* \rho^* \nabla^* c^*$$

$$-\Delta^* \mathbf{u}^* - \frac{1 + \nu}{1 - \nu} \nabla^*(\nabla^* \cdot \mathbf{u}^*) = -\eta^* \kappa^*(\rho^*)(\mathbf{u}^* - \mathbf{u}_c^*)$$

$$\frac{\partial c^*}{\partial t^*} - \Delta^* c^* = \alpha^*(\rho^*)\rho^* - c^*,$$

where we have defined the following non-dimensional groups of parameters:

$$\beta^* := \frac{\beta C \tau}{D}, \quad \eta^* := \frac{2(1 + \nu)\rho_0}{E\tau^2}$$

and the following non-dimensional functions:

$$p^*(\rho^*) := \frac{\tau}{D\rho_0} p(\rho_0 \rho^*), \quad \kappa^*(\rho^*) := \frac{\tau^2}{\rho_0} \kappa(\rho_0 \rho^*),$$

$$\alpha^*(\rho^*) := \frac{\rho_0 \tau}{C} \alpha(\rho_0 \rho^*).$$

If ρ_0 is thought of as the close-packing cell density, a possible intercellular pressure which behaves as described in Section 3 is

$$p^*(\rho^*) = \begin{cases} \varepsilon \rho^* & \text{for } 0 \leq \rho^* \leq 1 \\ \varepsilon \rho^* + b(\rho^* - 1)^3 & \text{for } \rho^* > 1 \end{cases} \qquad 0 < \epsilon \ll 1, \, 0 \leq b \ll 1$$

or, with weaker requirements on the regularity of the function p^*,

$$p^*(\rho^*) = \begin{cases} \varepsilon \rho^* & \text{for } 0 \leq \rho^* \leq 1 \\ \varepsilon + b(\rho^* - 1) & \text{for } \rho^* > 1 \end{cases}$$

and in this case $0 < \epsilon < b \ll 1$.

Moreover, we choose for $\kappa^*(\rho^*)$ a simple linear dependence on ρ^*:

$$\kappa^*(\rho^*) = \kappa^* \rho^*, \qquad \kappa^* > 0,$$

which actually implies a constant adhesiveness κ^* between ECs and ECM, and an elastic force proportional to the cell density.

Finally, according to the dynamics described in Section 3 (hypotheses i) and ii)) we use for $\alpha^*(\rho^*)$ the following expression:

$$\alpha^*(\rho^*) = \frac{\alpha_1}{1 + \alpha_2 \rho^{*2}}$$

14

with $\alpha_1 > 0$ and $\alpha_2 \geq 0$. Consequently, the production rate of chemoattractant is nearly independent of the cell density for low ρ^* and essentially vanishes for $\rho^{*2} \gg \frac{1}{\alpha_2}$.

Remark. Experimental measurements (see, *e.g.*, [21]) indicate that the order of magnitude of the diffusion coefficient of the chemical factor is $D \sim 10^{-7}$ cm^2/s, while its half-life is $\tau \sim 1$ h; consequently, the characteristic length ℓ turns out to be about 200 μm, in good agreement with the characteristic cord length experimentally observed.

Moreover, in order to estimate the parameter ρ_0 we assume that the close-packing cell density corresponds to the idealized situation in which each EC gets in touch with four other neighboring cells without overlapping. Here we specifically refer to the experimental assay by Serini *et al* [21]. Geometrically, regarding ECs as circles of constant radius, this configuration leads to a portion of plane surface covered by cells amounting to about 78% of the total surface of the ECM, which in turn implies for ρ_0 an order of magnitude of $2 \cdot 10^{-2}$ kg/m^2.

Finally, direct measurements of the parameter β, that in the model drives the networking via the chemotactic signaling, are not available. However, an indirect tuning of its non-dimensional counterpart β^* is possible on the basis of the total time (12-15 hours) needed for a complete formation of the structures.

References

[1] Ambrosi, D., Gamba, A. and Serini, G. (2004) "Cell directionality and chemotaxis in vascular morphogenesis", *Bull. Math. Biol.*, **66**(6), 1851-1873.

[2] Ambrosi, D., Bussolino, F. and Preziosi, L. (2005) "A review of vasculogenesis models", *J. Theor. Med.*, **6**(1), 1–19.

[3] Bischofs, I. B. and Schwartz, U. S. (2003) "Cell organization in soft media due to active mechanosensing", *PNAS*, **100**, 9274-9279

[4] Friedl, P. and Wolf, K. (2003), "Tumour-cell invasion and migration: diversity and escape mechanisms", *Nature Rev. Cancer* **3**, 362-374.

[5] Ferrenq, I., Tranqui, L., Vailhe, B., Gumery, P. Y. and Tracqui, P. (1997) "Modelling biological gel contraction by cells: mechanocellular formulation and cell traction quantification", *Acta Biotheoretica* **45**, 267-293.

[6] Gamba, A., Ambrosi, D., Coniglio, A., de Candia, A., Di Talia, S., Giraudo, E., Serini, G., Preziosi, L. and Bussolino, F. (2003) "Percolation, morphogenesis and Burgers dynamics in blood vessels formation", *Phys. Rev. Lett.* **90**, 11810/1-4.

[7] Galbraith, G. G. and Sheetz M. P. (1997) "A micromachined device provides a new bend on fibroblast traction forces", *PNAS Cell Biology*, **94**, 9114-9118.

[8] Gazit, Y., Berk, D. A., Leunig, M., Baxter, L. T. and Jain, R. K. (1995) "Scale-invariant behavior and vascular network formation in normal and tumor tissue", *Phys. Rev. E* **75**, 2428-2431.

[9] Grant, D., Tashiro, K., Segui-Real, B., Yamada, Y., Martin, G. and Kleinman, H. (1989) "Two different laminin domains mediate the differentiation of human endothelial cells into capillary-like structures in vitro", *Cell* **58**, 933-943.

[10] Gurtin, M. E. (1972) "The linear theory of elasticity", in *Handbuch der Physik*, Vol. VI a/2, Ed. by S. Flügge, Springer Verlag.

[11] Helmlinger, G., Endo, M., Ferrara, N., Hlatky, L., and Kain, R. K. (2000) "Formation of endothelial cell networks", *Nature* **405**, 139-141.

[12] Hendrix, M. J. C., Seftor, E. A., Meltzer, P. S., Gardner, L. M. G., Hess, A. R., Kirschmann, D. A., Sachatteman, G. C. and Seftor, R. E. B. (2001) "Expression and functional significance of VE-cadherin in aggressive human melanoma cells: Role in vasculogenic mimicry", *Proc. Nat. Acad. Sci.* **98**, 8018-8024.

[13] Kubota, Y., Kleinman, H., Martin, G., Lawley, T. (1988) "Role of laminin and basement membrane in the morphological differentiation of human endothelial cells into capillary-like structures", *J. Cell Biol.* **107**, 1589-1598.

[14] Kowalczyk, R. (2005) "Preventing blow-up in a chemotaxis model", *J. Math. Anal, Appl.*, **305**, 566-588.

[15] Manoussaki, D. (2003) "A mechanochemical model of angiogenesis and vasculogenesis", *ESAIM: Math. Model. Num. Anal.* **37**(4), 581-600

[16] Manoussaki, D., Lubkin, S. R., Vernon, R. B. and Murray, J. D. (1996) "A mechanical model for the formation of vascular networks *in vitro*", *Acta Biotheoretica* **44**, 271-282.

[17] Mariotis, A. J., Folberg, R., Hess, A., Seftor, E. A., Gardner, L. M. G., Pe'er, J., Trent, J. M., Meltzer, P. S. and Hendrix, M. J. C. (1999) "Vascular channel formation by human melanoma cells in vivo and in vitro: vasculogenesis mimicry", *Am. J. Path.* **155**, 739-752.

[18] Murray, J. D. and Oster, G. F. (1984) "Cell traction models for generation of pattern and form in morphogenesis", *J. Math. Biol.* **19**, 265-279.

[19] Namy, P., Ohayon, J. and Traqui, P. (2004) "Critical conditions for pattern formation and in vitro tubulogenesis driven by cellular traction fields", *J. Theor. Biol.* **227**, 103-120

[20] Ruhrberg, C., Gerhardt, H., Golding, M., Watson, R., Ioannidou, S., Fujisawa, H., Betsholtz, C., Shima, D. (2002) "Spatially restricted patterning cues provided by heparin-binding VEGF-A control blood vessel branching morphogenesis", *Gen. Devel.* **16**, 2684-2698.

[21] Serini, G., Ambrosi, D., Giraudo, E., Gamba, A., Preziosi, L. and Bussolino, F. (2003) "Modeling the early stages of vascular network assembly", *EMBO J.* **22**, 1771-1779.

[22] Sambeth, R. and Bamgaertner, A. (2001) "Autocatalytic polymerization generates persistent random walk of crawling cells", *Phys. Rev. Letters* **86**, 5196-5199.

[23] Tranqui, L. and Traqui, P. (2000) "Mechanical signalling and angiogenesis. The integration of cell-extracellular matrix couplings", *C.R. Acad. Sci. Paris, Science de la Vie* **323**, 31-47.

[24] Vailhe, B., Vittet, D. and Feige, J. J. (2001) "In vitro models of vasculogenesis and angiogenesis", *Lab. Investig.* **81**, 439-452.

[25] Webb, D. J. and Horwitz, A. F. (2003) "New dimensions in cell migration", *Nature Cell Biol.* **5** 690-692.

[26] Wolf, K., Mazo, I., Leung, H., Engelke, K., von Andrian, U. H., Deryugina, E. I., Strongin, A. Y., Bröcker, E. -B. and Friedl, P. (2003) "Compensation mechanism in tumor cell migration: mesenchymal-amoeboid transition after blocking of pericellular proteolysis", *J. Cell. Biol.* **160**, 267-277.
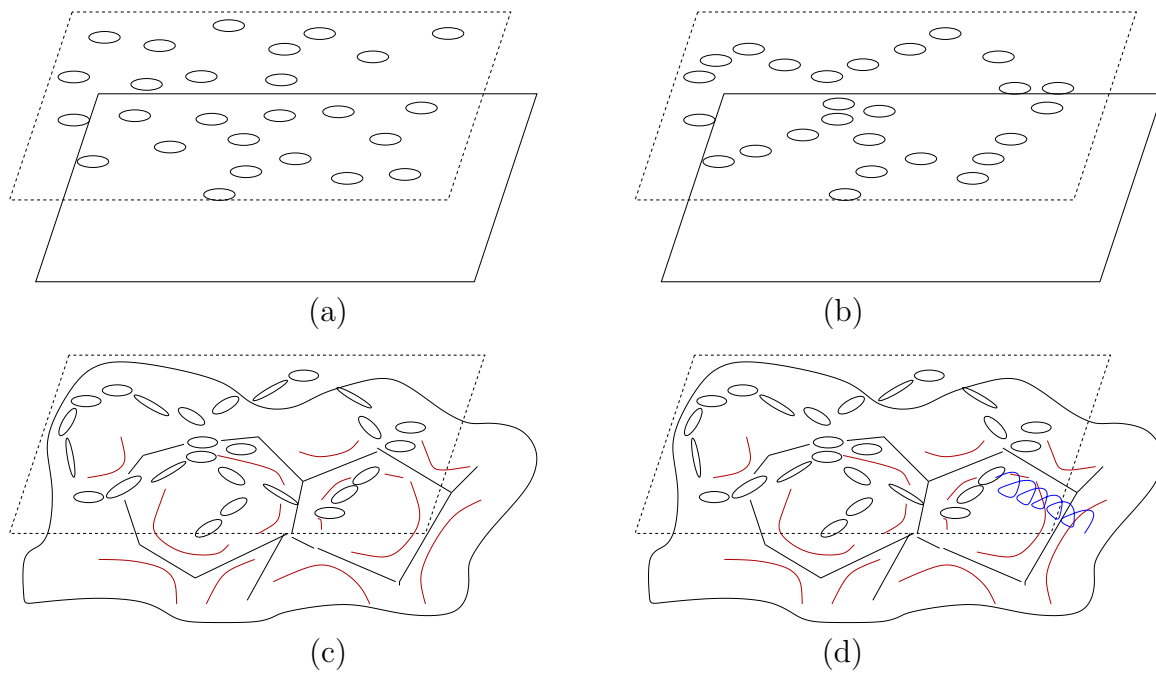
List of Figures

Fig. A.1. Random seeding of the cells (a), amoeboid cell migration along the gradient of the chemoattractant concentration (b), traction between the cellular layer and the gel (c). In Figure (d) is pictorially shown the spring ideally connecting the two layers.
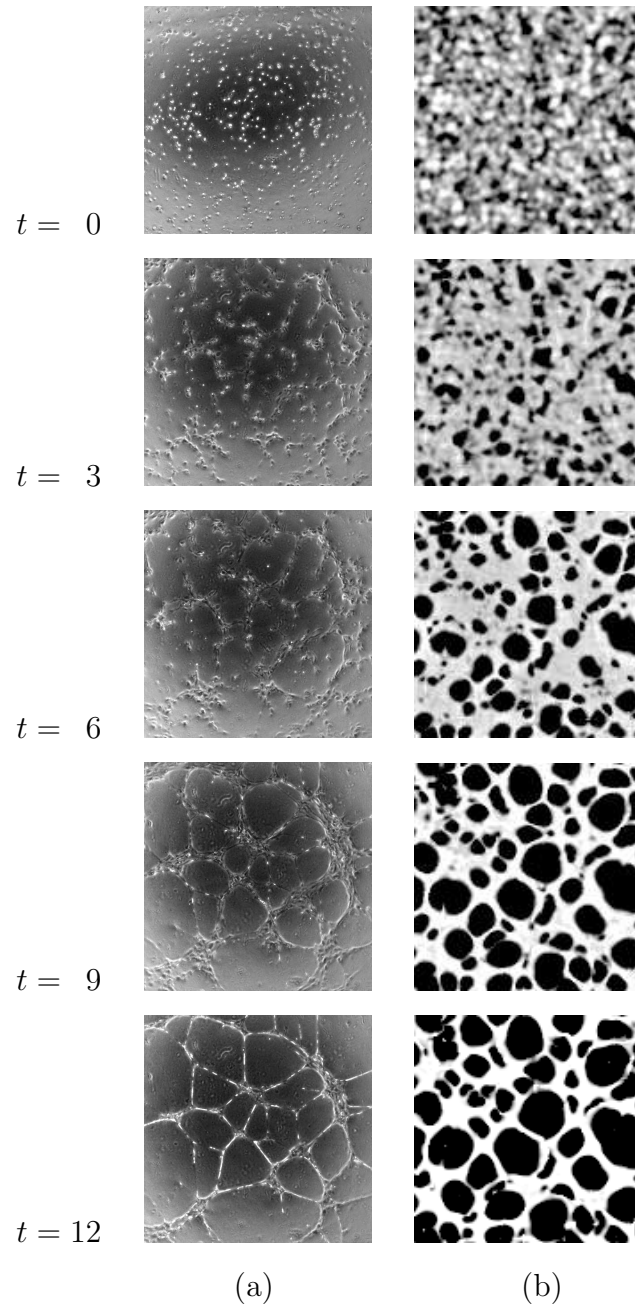
Fig. A.2. Formation of capillary networks: comparison between the experimentally observed (a) and the numerically predicted (b) morphology. The experimental pictures refer to a density of 125 cells/mm^2 of human microvascular ECs on a 4 mm^2 wide portion of Matrigel. Accordingly, the numerical simulation has been carried out starting from an initial condition of the form given in § 5 with $M = 800$, which closely mimics the real cell density. Numerical integration of the initial condition over the reference square allows to easily verify this claim, considering that the average cell mass is about $3 \cdot 10^{-11}$ kg. The non-dimensional time listed in the left column can be straightforwardly converted in dimensional form using the characteristic time $\tau = 1$ h.
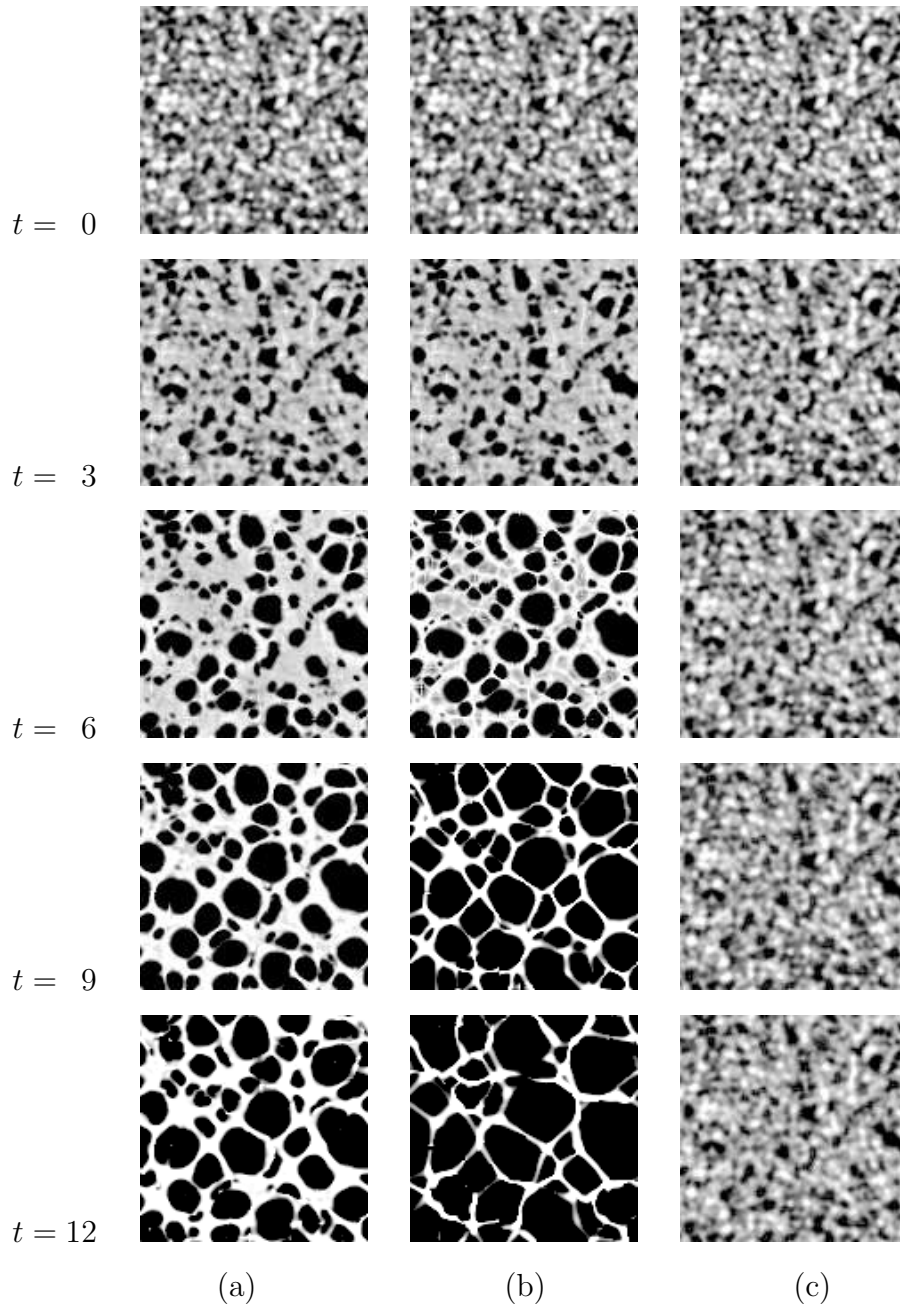
Fig. A.3. Influence of cellular adhesiveness to the substratum on network formation. When chemotactic attraction and mechanical interactions balance, a stable network structure arises (a). Instead, if adhesiveness is too low (b) or too strong (c) cords either rapidly form without giving rise to a stable structure or they do not form at all.
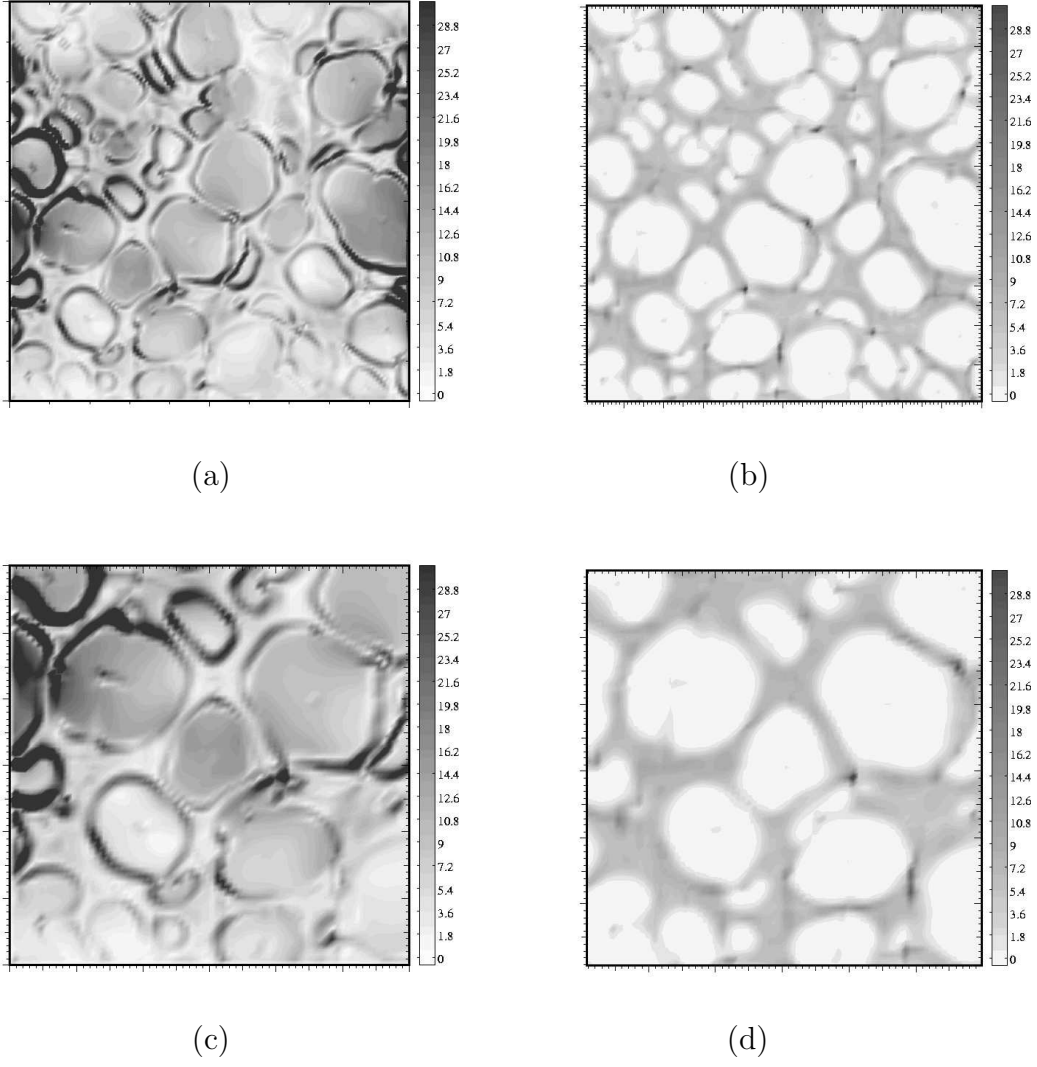
(a)

(b)

(c)

(d)

Fig. A.4. Plot of the norm of the ECM stress tensor (a) and the corresponding ECs density (b) at the final stage of network formation. A magnification of a portion of the domain is also shown (c, d). Stress values are here reported in dimensional form (obtained using $\nu = 0.2$ and $E = 10^3$ Pa as in Namy *et al.* [19]), corresponding to a maximum value of about 30 Pa.
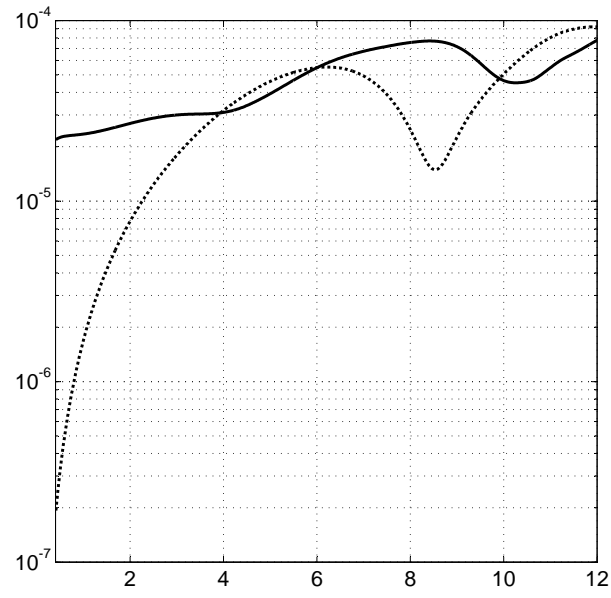
Fig. A.5. Plot in semi-logarithmic scale of the magnitude of the spatially-averaged chemotactic (solid line) and elastic (dotted line) forces versus time.